

A de novo protein catalyzes the synthesis of semiconductor quantum dots

Leah C. Spangler^{a,1} , Yueyu Yao^a, Guangming Cheng^b, Nan Yao^b, Sarangan L. Chari^{a,2}, Gregory D. Scholes^{a,2}, and Michael H. Hecht^{a,2}

Edited by Ivan Korendovych, Syracuse University, Syracuse, NY; received March 7, 2022; accepted October 28, 2022 by Editorial Board Member William F. DeGrado

De novo proteins constructed from novel amino acid sequences are distinct from proteins that evolved in nature. Construct K (ConK) is a binary-patterned de novo designed protein that rescues Escherichia coli from otherwise toxic concentrations of copper. ConK was recently found to bind the cofactor PLP (pyridoxal phosphate, the active form of vitamin B₆). Here, we show that ConK catalyzes the desulfurization of cysteine to H₂S, which can be used to synthesize CdS nanocrystals in solution. The CdS nanocrystals are approximately 3 nm, as measured by transmission electron microscope, with optical properties similar to those seen in chemically synthesized quantum dots. The CdS nanocrystals synthesized using ConK have slower growth rates and a different growth mechanism than those synthesized using natural biomineralization pathways. The slower growth rate yields CdS nanocrystals with two desirable properties not observed during biomineralization using natural proteins. First, CdS nanocrystals are predominantly of the zinc blende crystal phase; this is in stark contrast to natural biomineralization routes that produce a mixture of zinc blende and wurtzite phase CdS. Second, in contrast to the growth and eventual precipitation observed in natural biomineralization systems, the CdS nanocrystals produced by ConK stabilize at a final size. Future optimization of CdS nanocrystal growth using ConK—or other de novo proteins—may help to overcome the limits on nanocrystal quality typically observed from natural biomineralization by enabling the synthesis of more stable, high-quality quantum dots at room temperature.

de novo | quantum dots | biomineralization | protein design | binary patterning

De novo proteins are created in the laboratory from amino acid sequences that share no common ancestry with naturally evolved systems (1-7). One class of de novo proteins, pioneered by the Hecht group, comprises large combinatorial collections of sequences that are designed using a strategy that relies on a binary code for protein design. The binary code specifies the pattern of polar and nonpolar amino acids while allowing the exact identities of the individual side chains at each position to vary combinatorially. This approach facilitates the construction of libraries of proteins containing millions of different sequences. In particular, the binary code has produced several libraries of proteins that fold into 4-helix bundle structures (8–13). Importantly, these proteins were neither selected by nature nor do they have any relationship to natural biochemical pathways. Several proteins from this "alternate universe" of sequences have been shown to possess binding and/or catalytic activities both in vitro and in vivo (1, 5, 14-22). The occurrence of enzymatic activity is especially surprising as these sequences have no relationship to natural proteins and were not explicitly designed to have catalytic activity.

One particular de novo protein, called ConK (Construct K), was found to enable the survival of Escherichia coli in otherwise toxic concentrations of copper (1). While the mechanism of rescue was not fully elucidated and may be multifaceted, the resistance to a toxic metal suggests that ConK may have activities relevant to metal binding and/or sequestration.

Several naturally evolved metal sequestration and biomineralization pathways exist in bacteria that live in environments with high concentrations of toxic heavy metals (23–27). Generally, survival in toxic metal concentrations relies on a cellular response that sequesters the metal into a less toxic material, such as a metal sulfide. Biomineralization of metal sulfides has recently been implemented as a green, aqueous, and nontoxic route to produce functional materials, including semiconductor quantum dots (23, 28-30). In one case, the natural protein responsible for the biomineralization, cystathionine γ -lyase (CSE), was identified and purified for use in a clean single-protein approach for producing functional materials (28, 31-34). CSE is a pyridoxal phosphate (PLP)-dependent enzyme, which catalyzes the turnover of L-cysteine to reactive sulfur species in solution (35, 36).

We recently observed that ConK is also capable of binding PLP. This suggested the possibility of catalyzing the same desulfhydrase reaction used by CSE for metal

Significance

Combinatorial libraries of novel proteins can be designed from amino acid sequences with minimal similarity to those that evolved in nature. Because these novel proteins were not selected to perform life-sustaining functions, they represent a rich source of diversity for the isolation of new proteins capable of performing functions not seen in biology. Here, we show that a protein (ConK) isolated from one such combinatorial library facilitates the formation of cadmium sulfide quantum dots by catalyzing the production of a reactive sulfur species from the amino acid cysteine. These findings demonstrate that proteins not derived from biology can enable the production of functional materials, which, although not used to sustain biological organisms, have myriad uses in a range of technologies.

Author contributions: L.C.S., Y.Y., S.L.C., G.D.S., and M.H.H. designed research; L.C.S., Y.Y., G.C., and S.L.C. performed research; N.Y. contributed new reagents/analytic tools; L.C.S., Y.Y., G.C., N.Y., S.L.C., G.D.S., and M.H.H. analyzed data; and L.C.S. and M.H.H. wrote the paper.

Competing interest statement: The authors declare a competing interest. The authors have patent filings to disclose, A provisional patent application was filed 3/7/2022, Application No. 63/317,120.

This article is a PNAS Direct Submission. I.K. is a guest editor invited by the Editorial Board.

Copyright © 2022 the Author(s). Published by PNAS. This article is distributed under Creative Commons Attribution-NonCommercial-NoDerivatives License 4.0

¹Present address: Department of Chemical and Life Science Engineering, Virginia Commonwealth University, Richmond, VA 23229.

²To whom correspondence may be addressed. Email: hecht@princeton.edu, gscholes@princeton.edu, chari@princeton.edu.

This article contains supporting information online at https://www.pnas.org/lookup/suppl/doi:10.1073/pnas. 2204050119/-/DCSupplemental.

Published December 12, 2022.

sequestration. Here, we demonstrate that ConK indeed produces H_2S , which reacts with Cd^{2^+} in solution to produce CdS quantum dots. The mechanism of quantum dot formation shares similar chemistry to that employed by CSE: slow generation of H_2S in solution leading to controlled CdS quantum dot growth (37). This shared mechanism is surprising as ConK was not explicitly designed for function yet is capable of catalyzing the mineralization of CdS nanocrystals.

Results

The de novo protein ConK was originally identified by screening a library of binary-patterned de novo proteins for those that allow $E.\ coli$ to survive in otherwise toxic concentrations of copper (1). The binary patterning of this library typically generates 4-helix bundles, as illustrated in Fig. 1 A (9–11). Among these proteins, some bind the PLP cofactor and rescue strains of $E.\ coli$ that were deleted for natural enzymes that use PLP to catalyze essential metabolic reactions. ConK was one such de novo protein shown to bind PLP. The occurrence of PLP binding suggested that a ConK–PLP complex might be useful for processes catalyzed by natural enzymes employing the PLP cofactor.

One relevant PLP-dependent reaction is the desulfurization of cysteine into H₂S, pyruvate, and ammonia. In natural systems, this reaction is catalyzed by CSE and is an important step in methionine metabolism (39). This reaction is also important for the survival of microorganisms living in environments with high levels of toxic metals, such as cadmium. Recently, this reaction pathway, identified in an environmental strain of *Stenotrophomonas maltophilia*, was exploited to produce biomineralized metal chalcogenide quantum dots using natively expressed CSE (23, 29). Purified CSE was then used to catalyze the synthesis of a variety of metal chalcogenide nanocrystals, including CdS, CdSe, ZnS, CdZnS, and CuInS₂/ZnS core/shell nanocrystals (28, 30, 37, 40).

We hypothesized that the de novo protein ConK complexed with PLP might catalyze desulfurization of cysteine, thereby providing essential chemistry toward the formation of CdS nanocrystals. To verify PLP binding, purified ConK (0.25 mg/mL) was mixed with four times the molar concentration of PLP in 50 mM N-methylmorpholine (NMM) buffer. This led to the appearance

of an absorbance peak at 400 nm (Fig. 1 *C*), which is a well-known signature of PLP forming a Schiff base with lysine. When PLP was mixed with the related de novo protein, S824, the absorbance peak at 400 nm was absent, thereby confirming that the sequence and structure of ConK are required for PLP binding.

We confirmed PLP binding by ESI-MS. ConK and PLP were mixed at a ratio of 1:8 and then reacted with NaBH₄ to reduce the adduct, thereby stabilizing the otherwise reversible binding of PLP (41). Following reduction, ConK–PLP adducts were purified using reverse-phase HPLC. ESI-MS of the purified sample contained two series of peaks (*SI Appendix*, Fig. S1). Deconvolution revealed two populations: the first corresponded to a mass of 12.58 kDa, the expected mass of ConK. The other revealed a mass of 12.81 kDa, corresponding to the mass of ConK plus one PLP.

Knowing that ConK bound a single PLP, we next determined the lysine residue on ConK that forms the Schiff base. Using trypsin digestion to cleave at lysine and arginine residues, we obtained several peptides containing one or zero unmodified lysine. Analyzing peptides cleaved in the presence or absence of bound PLP revealed that PLP prevented cleavage at lysine 56 (SI Appendix, Fig. S3). Therefore, we hypothesized that PLP binds Lys56 to form the active site of ConK.

After confirming that ConK forms an adduct with PLP, we tested ConK for the desulfurization reaction, which converts cysteine to H₂S, ammonia, and pyruvate. If ConK catalyzes desulfurization, the enzymatically generated H₂S can subsequently react with Cd²⁺ in solution to form CdS quantum dots. Such CdS nanocrystals can also be stabilized by excess cysteine in solution, resulting in nanocrystal populations that are identifiable by characteristic signals in their absorbance and fluorescence spectra.

We tested ConK for its ability to catalyze the synthesis of CdS quantum dots by introducing L-cysteine (10 mM) and CdCl₂ (1 mM) to solutions containing ConK (0.2 mg/mL) and PLP (32 mM). For control experiments, we omitted either ConK or PLP. After incubation for 24 h, we monitored the appearance of absorbance peaks corresponding to CdS quantum dots (Fig. 2 A). Addition of CdCl₂ and excess cysteine to a solution containing ConK and PLP initially led to the appearance of a peak at 330 nm. This peak corresponds to the formation of a cysteine–aldimine

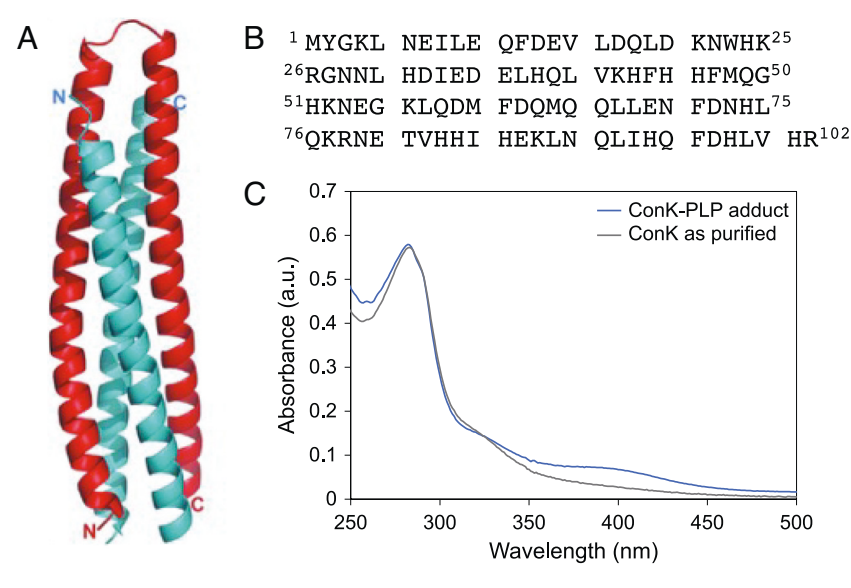


Fig. 1. De novo protein ConK and binding to PLP. (*A*) Crystal structure of WA20, a protein from a similar library as ConK. Adapted with permission from ref. 38. (*B*) Amino acid sequence of ConK. (*C*) Absorbance spectra of ConK before and after addition of PLP, confirming the formation of a PLP adduct by appearance of a peak at 400 nm.

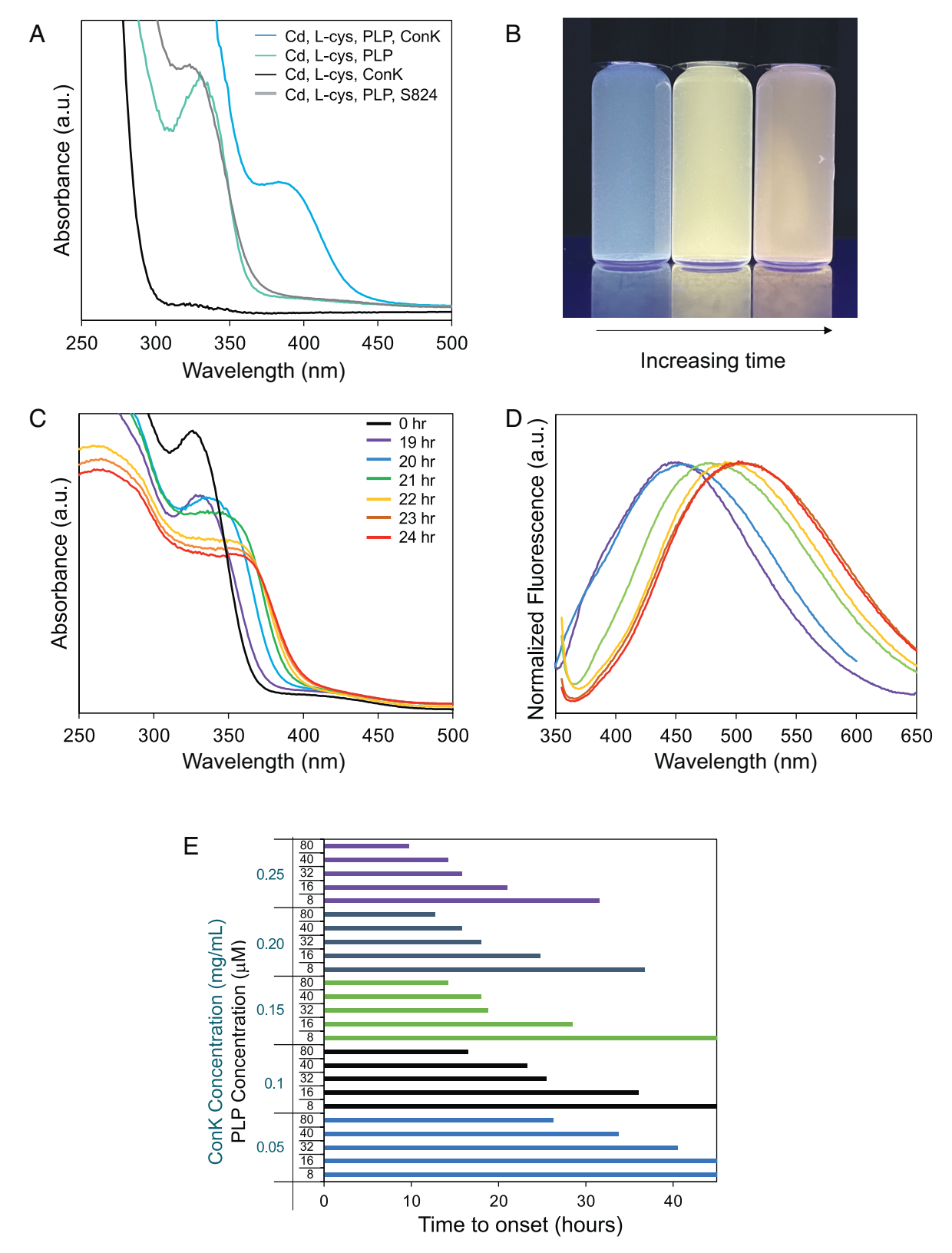


Fig. 2. Optical characterization of CdS quantum dots synthesized by ConK. (A) Absorbance spectra of solutions containing 1 mM CdCl₂ and 10 mM L-cysteine in 50 mM NMM buffer with 0.2 mg/mL ConK, 32 mM PLP, or both. A different binary-patterned protein (5824) was used as a negative control. The peak at 330 nm corresponds to cysteine-aldimine, a reactive intermediate that forms when PLP and L-cysteine are mixed in solution irrespective of ConK. The peak corresponding to CdS at 380 nm only forms when ConK and PLP are both present. (B) Solutions of three increasing sizes of CdS quantum dots formed by ConK show characteristic tunable fluorescence. Time course of (C) absorbance and (D) fluorescence spectra of CdS nanocrystal solutions grown with 0.25 mg/mL ConK and 32 mM PLP. (E) Required time for the onset of CdS nanocrystal formation vs concentrations of ConK and PLP.

intermediate, which forms spontaneously when cysteine and PLP are mixed in solution irrespective of the presence of protein (42). After 24 h, the solution containing ConK, PLP, CdCl₂, and

cysteine produced an additional peak around 380 nm, indicating the formation of CdS nanocrystals. Control solutions lacking PLP, ConK, CdCl₂, or cysteine failed to produce this peak. Importantly,

the same solution prepared with an alternative de novo protein, S824, shows no absorbance peak besides the 330-nm cysteine—aldimine intermediate, thereby confirming that ConK is required to generate quantum dots.

We also found that varying the incubation time allowed us to control the size of the CdS nanocrystals. This is illustrated by a change in the fluorescence of quantum dot solutions over time (Fig. 2 B). To determine the size of the nanocrystals, we incubated a solution containing CdCl₂, cysteine, ConK (0.2 mg/mL), and PLP (32 mM), and monitored absorbance and fluorescence for 24 h. At early times, the only observable peak was at 330 nm from the expected cysteine–PLP complex. However, after incubation for 19 h at 37 ° C, this peak decreased, with a concomitant increase of a peak at 340 nm, indicating the formation of CdS nanocrystals (Fig. 2 C).

Following their initial appearance, the CdS nanocrystals continued to grow for approximately 8 h, as shown by an absorbance peak that moved to longer wavelengths over time (Fig. 2 C). After 24 h, the peak stabilized at 380 nm, suggesting the nanocrystals grew to a fixed final size. The wavelength of the absorbance can be correlated to the size of the nanocrystals using the size-dependent Beer law calculation by Yu et al. (43). Based on the absorbance maximum, the CdS nanocrystals appear to shift in size from approximately 1.47 to 2.5 nm over the course of 24 h. The fluorescence peak maxima of the CdS nanocrystal populations, shown in Fig. 2 D, also shows a shifting wavelength over time. The size distribution of the resulting CdS nanocrystal populations can be evaluated by calculating the full width at half maximum (FWHM) of the fluorescence peak, which indicates population dispersity. The FWHM values, reported in SI Appendix, Table S1, range from 159 to 177 nm, consistent with relatively broad size distributions commonly observed for CdS nanocrystals synthesized via biomineralization (23, 44).

Not surprisingly, the time required to reach the onset of CdS nanocrystal formation depended on the concentration of ConK and PLP (Fig. 2 E). When higher concentrations of ConK (0.25 mg/mL) and PLP (80 μ M) were used, the appearance of a peak

at 340 nm occurred after only 10 h. For low concentrations of PLP and ConK (e.g., combinations of 8 to 16 mM PLP and 0.05 to 0.1 mg/mL ConK), we did not observe the onset of CdS quantum dots during the experimental time frame of 48 h. The long dwell time required for the formation of quantum dots suggests a slow generation rate of H_2S by ConK, which is not surprising for a de novo protein that was not explicitly designed for this function.

We further characterized the CdS nanocrystals using high-angle annular dark-field scanning transmission electron microscopy (HAADF-STEM) to measure the diameter, determine the CdS crystal phase, and confirm the chemical identity of each nanocrystal. We selected CdS nanocrystals from a sample with an absorbance peak at 370 nm, corresponding to approximately 3 nm in size, when calculated based on optical properties alone. A representative image of CdS nanocrystals is shown in Fig. 3 A. Despite their slightly irregular shape, the nanocrystal diameters are consistent with the size of -3 nm expected from the absorbance measurements. Lattice fitting measurements performed on several representative CdS nanocrystals (Fig. 3 B and C) identify the crystal structure of CdS to be zinc blende (SI Appendix, Table S2 and Fig. S2). The elemental composition of the nanocrystals was confirmed using energy-dispersive X-ray spectroscopy (EDS; Fig. 3 *D*) and shows clear peaks corresponding to both Cd and S. (Peaks corresponding to Si and Au are artifacts from the instrument and transmission electron microscope (TEM) grid.) The peak corresponding to Cl likely results from the cadmium chloride precursor.

The rate of CdS nanocrystal growth catalyzed by ConK is slower than the biomineralization catalyzed by the natural enzyme CSE. For CSE, the growth rate of CdS nanocrystals was limited by the amount of H_2S in solution and thus related to the enzymatic generation of H_2S (37). To quantify the amount of H_2S generated by ConK, we used the molecular probe 7-azido-4-methylcoumarin (AzMC), which reacts with H_2S to produce the fluorescent product 7-amino-4-methylcoumarine (AMC) (45). We measured the fluorescence of AMC, and thus generation of H_2S , for a solution

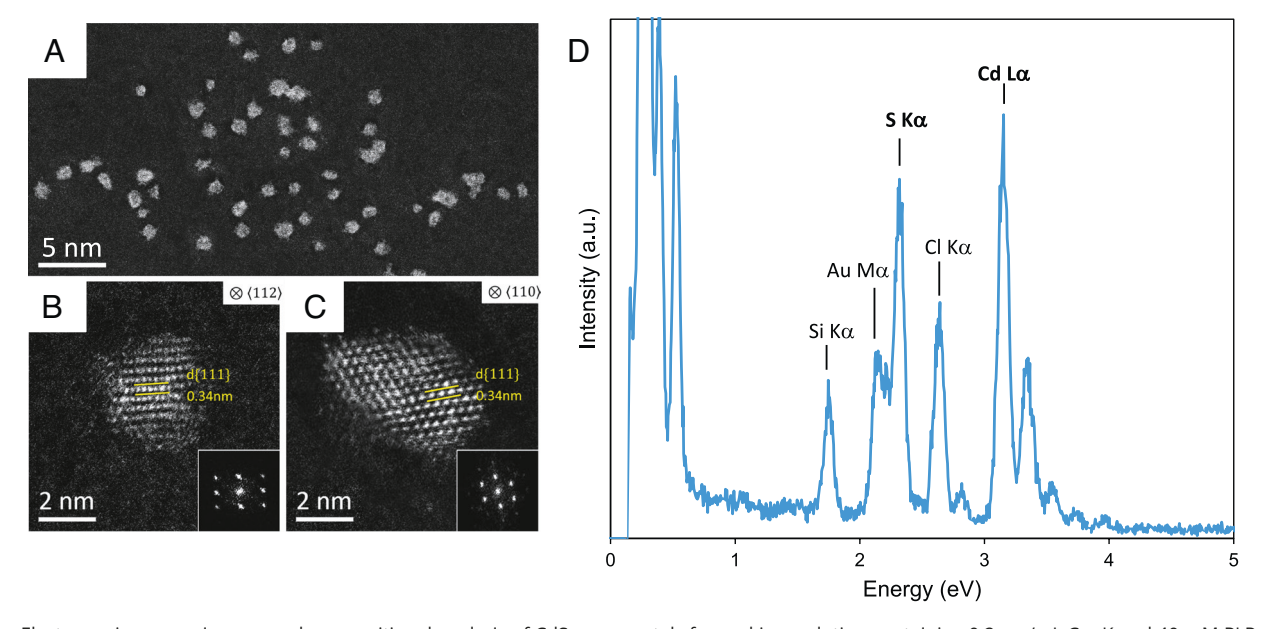


Fig. 3. Electron microscopy images and compositional analysis of CdS nanocrystals formed in a solution containing 0.2 mg/mL ConK and 40 mM PLP grown for 18 h. The absorbance peak in solution was 370 nm. (*A*) Representative HAADF-STEM image at low magnification. (*B* and *C*) High-magnification images of select CdS nanocrystals used for lattice fitting with inset showing corresponding FFT patterns. (*D*) EDS spectra collected from CdS nanocrystals confirming the presence of Cd and S.

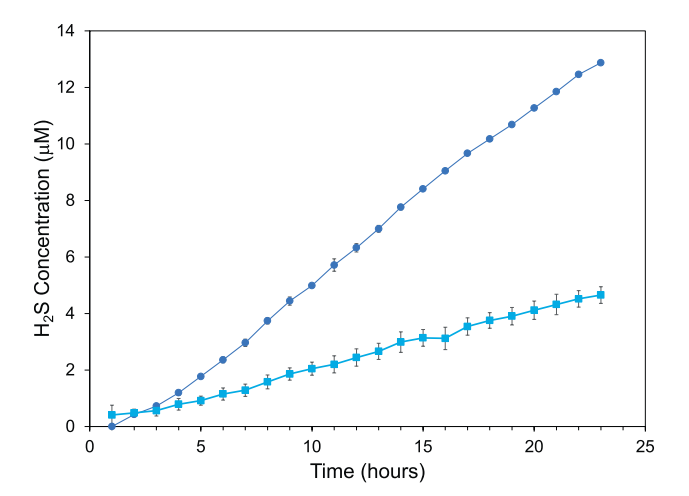


Fig. 4. Concentration of H₂S generated over 24 h in a solution containing 2.5 mM L-cysteine, 0.25 mg/mL ConK, and either 80 (circles) or 40 (squares) μM PLP. Error bars represent the standard deviation of three replicates.

containing L-cysteine (2.5 mM), ConK (0.25 mg/mL), and either 40 or 80 mM PLP. The concentration of H₂S increased linearly over time (Fig. 4) and was clearly dependent on the amount of PLP in solution. The sample with less PLP generated a much lower amount of H₂S, consistent with the longer dwell time required for CdS nanocrystal nucleation (Fig. 2 E). The overall rate of H₂S generation was slower than that observed previously for CSE: CSE generates 10 mM of H_2S in 1 h, while ConK required > 24 h (37).

The production of H₂S by ConK demonstrates that the mechanism of CdS QD formation is likely similar to that used by the natural protein CSE. This shared mechanism prompted us to investigate whether ConK and CSE share similarities in their active sites. Having previously identified Lys56 as the PLP-binding site, we set out to confirm that this was the catalytically active site by mutating this lysine to arginine. The mutated protein, K56R, showed no change in expression or purification. However, K56R did not produce absorbance peaks characteristic of CdS QD formation (Fig. 5 *A*), thereby demonstrating that Lys56 is essential for activity.

To study the active site of ConK in the absence of an experimentally determined structure, we used AlphaFold (46) to predict the structure. Because ConK appears to oligomerize in solution (vide infra), we modeled the structure as either a monomer or a dimer. In the AlphaFold prediction, Lys56 occurs in a semiexposed pocket in the 2nd interhelical turn of the protein. Because of the location of this turn, this binding pocket is the same in both the monomeric and dimeric states (Fig. 5 B). We also identified 3 relevant proximally close amino acids, His43, His46, and Phe47. Aromatic amino acids are often observed in PLP-binding sites because they stabilize the pyridine ring through π -stacking (35). Similarly, histidines have also been shown to stabilize the pyridine ring by forming an H-bond with nitrogen (47). The proximity of both Phe and His side chains is consistent with natural PLPdependent enzyme active sites. We note that although the active site of ConK shares several features with the PLP-binding sites in CSE, such as forming a Schiff base with lysine and the presence of aromatic amino acids, the sequence and structure of the active site pocket are dramatically different. This is expected as ConK has no evolutionary ancestry and was isolated from a library of semirandom de novo sequences.

To assess the stereoselectivity of the ConK catalytic site, we replaced L-cysteine with D-cysteine and monitored the formation of CdS nanocrystals. Using D-cysteine led to an absorbance peak corresponding to CdS quantum dots (Fig. 6 A), indicating that D-cysteine can also be turned over to H₂S by ConK. Notably, cysteine plays a dual role in our system, acting as both a reactant and a capping ligand that stabilizes the quantum dot surface. We found that the D-isomer can also serve as a capping agent. Following filtration using a 10-kDa MWCO filter to remove cysteamine adducts, the resulting CdS quantum dot solutions were assayed for chirality by CD spectroscopy. We found the signal to be exactly opposite when using D-cysteine (Fig. 6 B), indicating that D-cysteine acts as a mirror image capping ligand on the surface of the CdS quantum dot (48-50).

Having shown that ConK catalyzes the formation of CdS quantum dots, we sought to characterize the solution properties of this de novo protein. The secondary structure of ConK was assessed by circular dichroism (CD) spectroscopy. As shown in *SI Appendix*,

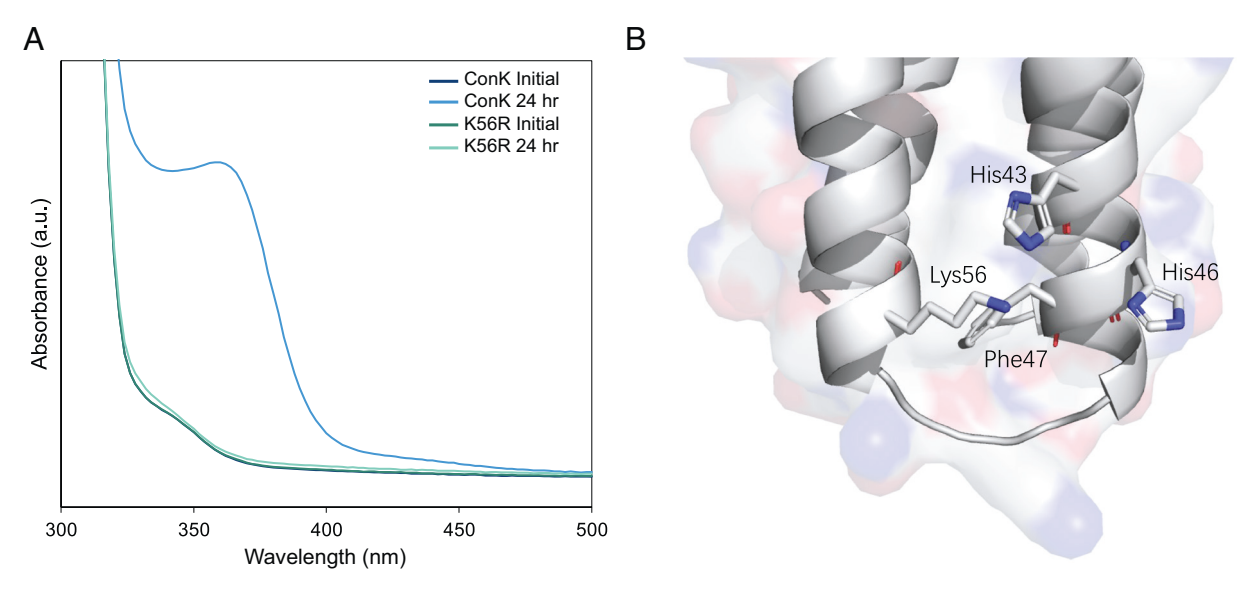


Fig. 5. Mutagenesis studies determine the active site of ConK. (A) QD synthesis using either ConK or the mutant K56R demonstrate loss of desulfurization activity when the lysine responsible for PLP binding is mutated to arginine. (B) Structural prediction of the active site-binding pocket around Lys 56 showing proximity with Phe and His residues.

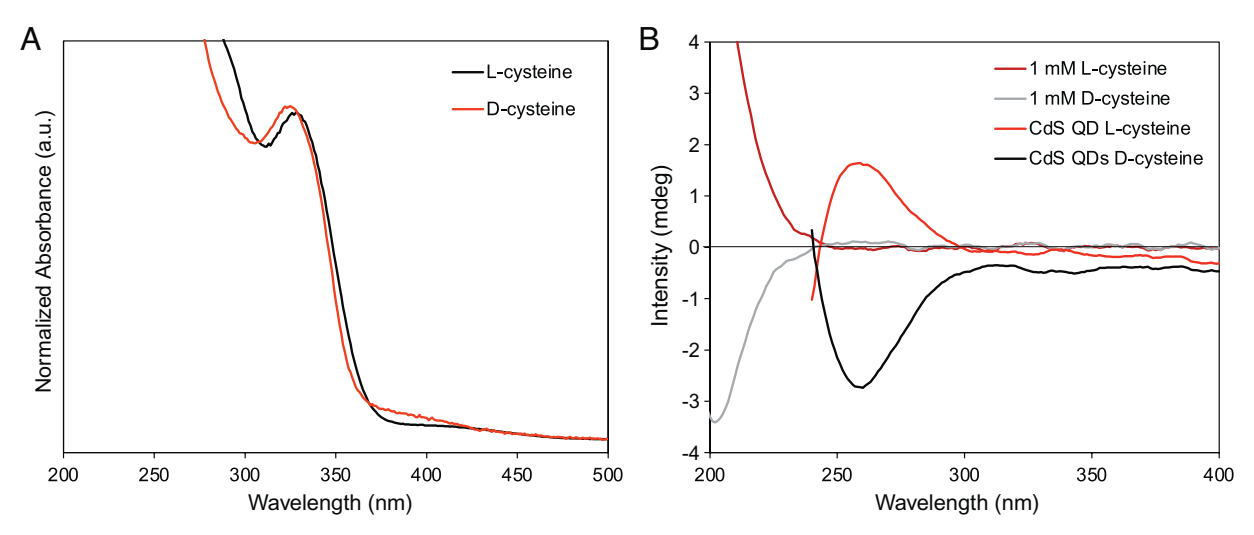


Fig. 6. Analysis of chiral CdS quantum dots synthesized using L- or D-cysteine. (A) Absorbance spectra and (B) CD spectra of CdS quantum dots. The CD spectra are opposite in sign caused by the chirality of the cysteine capping ligand. CD spectra of L-cysteine and D-cysteine alone are shown as controls to demonstrate they give no signal in the excitonic region (>250 nm).

Fig. S4, the CD spectrum shows minima at 208 and 222 nm, typical of α -helical proteins. This is not surprising and has been observed previously for many binary-patterned proteins designed to fold into 4-helix bundles (8–13). The CD spectrum of ConK bound to PLP is nearly identical to that of the apoprotein, indicating that addition of the cofactor does not significantly alter the overall structure of the protein.

The oligomeric state of ConK was assessed by gel filtration chromatography. The observed elution volume corresponds to a mass of approximately 40 kDa (SI Appendix, Fig. S5D). Since the covalent molecular mass of ConK is 12.58 kDa (confirmed by ESI-MS; SI Appendix, Fig. S5 A and B), this result indicates that ConK forms oligomers in solution. Next, we used native PAGE to compare ConK with the related de novo protein, S824, which has approximately the same covalent molecular weight but forms monomers in solution, with a 3D structure solved previously by nmR (11). As shown in *SI Appendix*, Fig. S5G, ConK migrates more slowly than S824, consistent with the formation of oligomers. Finally, the formation of oligomers was confirmed using analytical ultracentrifugation. Analysis of the data showed two main coefficients of separation (SI Appendix, Fig. S5E). The largest peak corresponds to a molecular weight of 39.5 kDa, consistent with the results from gel filtration, and suggest an oligomeric state approximately three times the covalent molecular weight of ConK. A small fraction of ConK appears to exist as a monomer (4%). Another smaller but broad peak corresponding to 131 kDa was also present, likely due to the formation of some larger aggregates. Such aggregates appear to contain close to a third of the total protein (32%); however, the time needed for analytical ultracentrifugation is >12 h, so additional aggregation may occur due to the conditions of the experiment.

To determine whether mutation of Lys56 affects oligomerization, we compared ConK and the mutated protein, K56R, by exclusion chromatography (*SI Appendix*, Fig. S6). Observation of the same characteristic peaks demonstrates that replacement of the lysine side at position 56 abrogates catalytic activity without perturbing the oligomeric state of the protein.

Discussion

To the best of our knowledge, ConK is the first de novo protein reported to catalyze the synthesis of semiconductor quantum dots.

ConK was neither explicitly designed for this function nor was it selected by eons of natural evolution, so this catalytic capability is remarkable. ConK was also found previously to confer survival to *E. coli* grown in otherwise toxic concentrations of copper. The proposed mechanism at that time was not H₂S generation but instead binding of copper ions to histidine residues located on ConK (1). It is possible that ConK also binds cadmium in a similar way, but the production of sulfur dominates, resulting in the formation of CdS quantum dots as opposed to a cadmium precipitate. In vivo, it is possible that both mechanisms act to rescue *E. coli* from copper toxicity as both have been observed as methods for neutralizing toxic heavy metals in natural systems, including bacteria, plants, and yeast (25–27). Future work will examine whether sulfur production plays a role in copper survival by identifying inorganic precipitates as copper, CuS, or a mixture of both.

The turnover of cysteine to $\rm H_2S$ is slow, but this is not surprising for a de novo protein that was neither designed for a specific function nor subjected to evolution—either in vivo or in vitro. The dependence on the concentration of protein is expected and typical. The dependence on PLP concentration is also expected as this cofactor is required for the reaction. Because the reaction is slow, the increase in the reaction rate with PLP concentration may simply result from PLP spending less time diffusing to the active site. The reaction rate dependence on PLP is unique to ConK. Naturally evolved enzymes, such as CSE, bind PLP more strongly and likely retain the bound cofactor after each catalytic step.

Once nucleated, the nanocrystal growth rate appears to depend on the production of H₂S in solution. H₂S-dependent growth is similar to that catalyzed by the naturally evolved protein CSE (37). The growth rate can be quantified by calculating the shift in absorbance peak versus time. For a solution containing 0.25 mg/ mL ConK and 80 mM PLP, the CdS absorbance peak shifts at approximately 0.15 nm/min (SI Appendix, Fig. S7), while the rate of H₂S generation is approximately 0.1 mM H₂S/min (Fig. 4). The relationship between the absorbance peak shift, or nanocrystal growth, and H₂S generation rate is approximately 3:2. This same 3:2 relationship was also observed for CdS quantum dots biomineralized using the natural protein CSE. While the overall synthesis catalyzed by CSE was faster (37), the shared ratio between the quantum dot growth rate and H₂S production suggests a similar growth mechanism that depends on the rate of H₂S generation in solution.

While CdS nanocrystal growth is similar following nucleation, there remains a striking difference between ConK and natural systems in the time required to nucleate CdS nanocrystals. In the natural system using CSE, an absorbance peak corresponding to CdS quantum dots appears in less than 30 min. In contrast, for ConK, nucleation is not observed for at least 10 h. The long dwell time may simply result from the slow generation of H₂S: Nucleation can occur only after H₂S is present at a concentration that causes supersaturation of CdS.

Another cause for the slow nucleation may be competition for cysteine. In addition to serving as the reactive precursor for H₂S and capping agent, cysteine is also a strong chelator of Cd²⁺ and thereby impacts the supersaturation conditions required for nucleation. Specifically, cysteine likely mediates the formation of the small CdS complexes that serve as nucleation points for nanocrystal growth (51). Cysteine will also react with excess PLP in solution to form cysteine-aldimine complexes, which introduces additional competition for cysteine and will inhibit the formation of small CdS complexes needed for nucleation. This effect is not observed in natural systems where PLP is bound tightly to the enzyme and excess PLP is not required to drive the reaction.

Slow H₂S production and delayed nucleation likely affect the properties of the resulting CdS nanocrystals. For example, the calculated FWHM values for CdS nanocrystals synthesized by ConK increased with growth time, demonstrating size broadening behavior. Size broadening tends to indicate growth via Ostwald ripening (52). Previous biomineralization routes demonstrated size focusing behavior (37). As previously discussed, the availability of cysteine will affect the supersaturation conditions required to nucleate particles (51). This may also modify the growth behav-

Despite the differences in growth, CdS QDs formed by ConK appear similar in their optical properties to those synthesized using naturally occurring enzymes such as CSE. For a quantitative comparison, we measured the photoluminescent quantum yield (PLQY) of our CdS QDs immediately following synthesis. We found that our particles have a PLQY of 0.3%. While low, this value is consistent with other reported CdS QDs synthesized under mild aqueous conditions: The current record of PLQY for biogenically produced CdS QDs is 2.3% (53). PLQY is likely low compared with chemically synthesized CdS QDs as a result of using cysteine as a capping agent, which can quench nanocrystal fluorescence (54). Future work will aim to improve PLQY using core/shell growth, optimization of growth conditions such as pH, and modifying capping ligands to other small molecules. Moreover, variants of ConK, or other binary-patterned de novo proteins from similar combinatorial libraries, can be tested for enhanced QD performance.

Another major difference between CdS quantum dots grown using ConK versus natural systems such as CSE is the structure of the resulting nanocrystals. A mixed distribution of crystal phases is commonly observed for CdS nanocrystals synthesized at room temperature via natural biomineralization routes (23). In contrast, for synthesis using ConK, only one phase of CdS, zinc blende, was observed. The dominance of zinc blende CdS is striking and indicates that the slow growth using ConK favors more controlled crystallization. This suggests that ConK could produce higherquality crystallites at room temperature than those previously achieved by natural proteins.

An additional advantage of the slow growth facilitated by ConK is that after several hours, the nanocrystals settle at a specific size (~3 nm). In contrast, nanocrystals synthesized by the natural protein CSE continue to grow until they aggregate and precipitate from solution. Such aggregation is not desirable as it leads to loss of quantum confinement and the associated optical properties. ConK is able to restrict growth to a final size because of the slow rate of H₂S generation. The slower production of H₂S allows the size to stabilize around the time when catalysis of the reactive precursor ends. Catalysis likely stops due to degradation of PLP, freely available L-cysteine, or the protein itself. While protein degradation is often viewed in a negative context, here it is an advantage as quenching of the QD reaction is not required and occurs spontaneously.

The slow kinetics of ConK are expected as the protein was designed in the laboratory based on a specified protein structure motif rather than a specified function. Following design, ConK was not evolved to produce H₂S more efficiently. The lack of evolution is evident when comparing ConK to the naturally evolved protein, CSE. For CSE, the binding of PLP causes aromatic amino acids to approach the PLP-lysine complex, thereby favoring cysteine binding and subsequent formation of H₂S (35). In contrast, the unevolved ConK protein is unlikely to undergo this structural reorganization, and so, the overall kinetics would be slower. Future work will investigate how these neighboring aromatic amino acids affect the rate of reaction.

The mechanism of nanocrystal formation observed here stands in stark contrast to biomineralization mechanisms that utilize strong metal-binding proteins to control nanocrystal size, shape, and crystal phase. Such metal-binding proteins facilitate the formation of nanocrystals at a specific size (i.e., 2.5 nm only) by physically inhibiting crystal growth on the surface. However, such systems do not allow for controlled growth to the range of sizes (2 to 5 nm) observed with ConK. Continuous growth by ConK is facilitated by the continuous generation of reactive precursor that eventually tapers off, limiting growth to a final size. This slow growth could be advantageous for biological detection of contaminants or when used as a biological probe.

Conclusion

Here, we present the synthesis of CdS nanocrystals using a protein designed de novo. ConK catalyzes the formation of quantum dots through the desulfurization of cysteine to produce H₂S, which subsequently reacts in solution with CdCl₂ to form CdS nanocrystals. Cysteine also acts as a capping agent, stabilizing size-controlled populations of nanocrystals. The particle size, crystal phase, and composition of CdS nanocrystals were confirmed using HAADF-STEM imaging. The active site of cysteine desulfurization was identified at Lys56, where PLP forms a Schiff base that is likely stabilized by a neighboring aromatic residue, Phe47. ConK was found to use either L-cysteine or D-cysteine as a reactive precursor, resulting in the possibility of controlled formation of chiral CdS quantum dots. The kinetics of H₂S generation by ConK were found to be ~0.1 mM H₂S/min, resulting in an onset of CdS nucleation of >10 h, depending on the concentration of ConK and PLP. While nanocrystal formation by ConK is slower than that by naturally derived biogenic routes, the slow rate may be advantageous for halting growth at a desired nanocrystal size and controlling the crystal phase, thereby facilitating improved stability and quality for room temperature syntheses of quantum dot nanocrystals.

Materials and Methods

Expression and Purification of ConK and mutants. ConK and K56R were expressed using recombinant E. coli as described previously (1). The amino acid sequence of ConK is shown in Fig. 1 B. The plasmid encoding ConK was transformed into BL21 (DE3) E. coli from NEB. Following transformation, cells were plated onto LB supplemented with chloramphenicol (30 µg/mL) and grown overnight at 37 °C. A single colony was then used to inoculate a 2 L volume of LB broth supplemented with 30 $\mu g/mL$ chloramphenicol. This culture was grown at 37 °C until the cell concentration reached an OD $_{600}$ of about 0.5. At this time, IPTG (final concentration of 100 μ M) was added to induce protein expression, followed by incubation at 18 °C overnight. Following overexpression, cells were recovered by centrifugation at 3,000 \times g and frozen at -20 °C for later use.

Immediately prior to purification, frozen cell pellets containing overexpressed ConK were thawed and resuspended in 25 mL of 50 mM Tris and 300 mM NaCl (buffer A) at 4 °C for 30 min. The resuspended cells were then sonicated on ice using a probe-tip sonicator for a total of 4 min (pulse 10/50 s on/off) and 30% amplitude. Next, the lysate was clarified by centrifugation at 35,000 \times g for 30 min to separate the soluble overexpressed proteins from cell debris. The protein-rich supernatant was filtered using 0.22- μ M PES membrane syringe filters.

ConK was purified using immobilized metal affinity chromatography (IMAC) followed by size-exclusion chromatography (SEC). While ConK does not carry a canonical histidine tag (6× His) typically required for IMAC, its sequence contains a high percentage of histidine (ca. 14%) enabling nickel binding. First, the filtered supernatant containing ConK was applied to a 5-mL HisTRAP column (GE Healthcare) and equilibrated with five column volumes of running buffer containing 50 mM Tris and 300 mM sodium chloride at pH 7.5. A second wash step using five column volumes of 50 mM imidazole, 50 mM Tris, and 300 mM NaCl at pH 8 removed any nonspecifically bound proteins. ConK was then eluted using 375 mM imidazole, 50 mM Tris, and 300 mM NaCl. The eluates were analyzed by SDS-PAGE, and the appropriate fractions were pooled and further purified by SEC on a HiLoad Superdex 75 26/600 column (GE Healthcare). SEC also removes imidazole from the IMAC stage. This two-stage process typically yields proteins of greater than 95% purity, as assessed by SDS-PAGE. ESI-MS measurements were performed on 10-uL of protein following separation on the HPLC (Agilent 6220 accurate-mass time-of-flight LC/MS). Further characterization of ConK oligomerization was performed using analytical ultracentrifugation (Optima AUC from Beckman Coulter Life Sciences with absorbance and interference detection modules).

PLP Binding and Trypsin Digestion. Purified ConK (30 μM) was incubated with PLP at a 1:8 ratio in HEPES buffer (25 mM HEPES and 300 mM NaCl, pH 7.4) at 37 °C for 18 h. The PLP adducts were reduced in neutral conditions by addition of 10 mM NaBH₄, and the reaction was allowed to proceed for 30 min at room temperature. Trypsin-ultraTM, mass spectrometry grade (New England BioLabs) was added in a 1:40 protease:substrate ratio. Following 4-h incubation at 37 °C, RP-HPLC was used to separate peptide fractions. The RP-HPLC method consisted of a gradient from 3%:97% (v/v) $\rm H_2O$:acetonitrile to 60%:40% (v/v) $\rm H_2O$:acetonitrile in 25 min. ESI-MS peptide mass analysis was then performed on $\rm 10$ -μL injections of fractions separated by RP-HPLC to identify the peptide with an increase in mass, which corresponded to the mass of a reduced PLP adduct (230 Da).

Mutation Studies on Conk. PCR mutagenesis was performed by whole-plasmid PCR with Q5 high-fidelity polymerase (New England BioLabs) followed by PCR purification (Qiagen) and treatment with the Kinase/Ligase/DpnI Mix (New England BioLabs). The primers were made by Sigma-Aldrich with the following sequences: 5'-CGAGGGCCGCCTGCAGGACA-3' (K56R_For) and 5'-TTCTTGTGGCCCTGCATAAAGTGG-3' (K56R_Rev). The resulting plasmids were confirmed by sequencing (Genewiz) before being transformed into BL21 (DE3) *E. coli* for expression.

Synthesis of Quantum Dots. We initiated quantum dot synthesis by preparing a solution of 1 mM cadmium chloride (99%, Sigma-Aldrich) and 10 mM L-cysteine (>97%, Sigma-Aldrich) in 50 mM nmM at pH 7.5. To this solution, we added various concentrations of ConK (0 to 0.25 mg/mL) followed by PLP (0 to

 K. J. Hoegler, M. H. Hecht, A de novo protein confers copper resistance in Escherichia coli: Novel protein confers copper resistance. Protein Sci. 25, 1249–1259 (2016). $80~\mu M)$, which initiates the biomineralization process. Following addition of PLP, the reaction mixture was placed in an 37 °C incubator with shaking for 0 to 48 h.

Quantification of H2S using the AzMC Assay. We quantified the rate of H_2S generation using an adapted version of the AzMC assay initially developed by Thorson et al. (45). In brief, AzMC (Sigma-Aldrich, 97%) was dissolved in DMSO and used at a final concentration of 10 μ M. An assay solution was prepared containing 50 mM nmM, 0.25 mg/mL ConK, and either 40 or 80 μ M PLP. We pipetted 180 μ L of this assay solution into a 96-well plate. We then added 10 μ L AzMC and 10 μ L sample to each well. The sample consisted of either L-cysteine (2.5 mM final concentration, Sigma, >98%) or various concentrations of NaHS (Sigma-Aldrich), which were used to produce a calibration curve spanning 1 to 100 μ M. The samples were incubated at 37 °C and measured every 30 min over 24 h. Each sample was prepared in triplicate.

Characterization of Quantum Dots. Absorbance measurements were collected on a Cary 6000 UV/Vis spectrometer with an integrating sphere attachment (Agilent). The cuvette (Quartz Fluorometer Cell, 10-mm path length; Starna) was placed in the center of the integrating sphere to reduce scattering effects. Fluorescence measurements were recorded on a QuantaMaster (HORIBA) using an excitation wavelength of 340 nm. The AzMC assay and 96-well plate screening of nanocrystal solutions were recorded using a Tecan plate reader.

For CD measurements, the quantum dot solution was concentrated using a centrifugal concentrator with a 3.5-kD cutoff membrane to remove all the small molecules and PLP complexes. To prevent possible aggregation of the quantum dots on the membrane, the membrane was pretreated with the appropriate enantiomer of cysteine (10 mM). The quantum dot concentrate was reconstituted in a 1 mM solution of the appropriate cysteine enantiomer to avoid the loss of the capping cysteine ligand through dynamic exchange. This buffer exchange process was repeated no fewer than four times. CD measurements were performed using a 1-mm path length cuvette at room temperature (Chirascan CD Spectrometer; Applied Photophysics).

Conventional transmission electron microscope (TEM) imaging, atomic resolution high-angle annular dark-field (HAADF)-STEM imaging, and atomic-level EDS mapping were performed on a double Cs-corrected FEI Titan Cubed Themis 300 scanning/transmission electron microscope (S/TEM) equipped with an X-FEG source and a super-X energy-dispersive spectrometer. The system was operated at 200 kV.

Data, Materials, and Software Availability. All study data are included in the article and/or *SI Appendix*.

ACKNOWLEDGMENTS. We thank Dr. Venu Gopal Vandavasi for assistance with the analytical ultracentrifugation measurements performed in the Biophysical Chemistry core facility at the Department of Chemistry, Princeton University. We also thank Dr. John Eng and the Mass Spectrometry core facility. We wish to acknowledge discussions and help from Prof. Wayne Patrick, Victoria University of Wellington, New Zealand. The authors acknowledge the use of Princeton's Imaging and Analysis Center, which is partially supported through the Princeton Center for Complex Materials (PCCM), a National Science Foundation (NSF) MRSEC program (DMR-2011750). This work was supported by the NSF grants MCB-1947720 and MCB-1409402 to M.H.H. Additional funding was provided by the Princeton University Writing Center and CIFAR (Canadian Institute for Advanced Research). Dr. Gregory Scholes is CIFAR fellow.

Author affiliations: ^aDepartment of Chemistry, Princeton University, Princeton, NJ 08544; and ^bPrinceton Institute for the Science and Technology of Materials, Princeton University, Princeton, NJ 08544

C. Tommos, J. J. Skalicky, D. L. Pilloud, A. J. Wand, P. L. Dutton, De novo proteins as models of radical enzymes. Biochemistry 38, 9495–9507 (1999).

P.-S. Huang, S. E. Boyken, D. Baker, The coming of age of de novo protein design. Nature 537, 320–327 (2016).

B. Kuhlman et al., Design of a novel globular protein fold with atomic-level accuracy. Science 302, 1364–1368 (2003).

D. A. Moffet, M. H. Hecht, De novo proteins from combinatorial libraries. Chem. Rev. 101, 3191–3204 (2001).

J. Kaplan, W. F. DeGrado, De novo design of catalytic proteins. Proc. Natl. Acad. Sci. U.S.A. 101, 11566–11570 (2004).

I. V. Korendovych, W. F. DeGrado, De novo protein design, a retrospective. Quart. Rev. Biophys. 53, e3 (2020)

M. H. Hecht, A. Das, A. Go, L. H. Bradley, Y. Wei, *De novo* proteins from designed combinatorial libraries. *Protein Sci.* 13, 1711–1723 (2004).

Y. Wei, Stably folded de novo proteins from a designed combinatorial library. Protein Sci. 12, 92–102 (2003).

S. Kamtekar, J. Schiffer, H. Xiong, J. Babik, M. Hecht, Protein design by binary patterning of polar and nonpolar amino acids. Science 262, 1680–1685 (1993).

- 11. Y. Wei, S. Kim, D. Fela, J. Baum, M. H. Hecht, Solution structure of a de novo protein from a designed combinatorial library. Proc. Natl. Acad. Sci. 100, 13270-13273 (2003).
- L. H. Bradley, R. E. Kleiner, A. F. Wang, M. H. Hecht, D. W. Wood, An intein-based genetic selection allows the construction of a high-quality library of binary patterned de novo protein sequences. Protein Eng. Des. Sel. 18, 201-207 (2005).
- C. Karas, M. Hecht, A strategy for combinatorial cavity design in de novo proteins. Life 10, 9 (2020).
- M. A. Fisher, K. L. McKinley, L. H. Bradley, S. R. Viola, M. H. Hecht, De novo designed proteins from a library of artificial sequences function in *Escherichia coli* and enable cell growth. *PLoS One* **6**, e15364 (2011).
- A. Das, Y. Wei, I. Pelczer, M. H. Hecht, Binding of small molecules to cavity forming mutants of a *de novo* designed protein: Binding of small molecules to a designed protein. *Protein Sci.* 20, 702–711 (2011).

 I. Cherny, M. Korolev, A. N. Koehler, M. H. Hecht, Proteins from an unevolved library of *de novo*
- designed sequences bind a range of small molecules. ACS Synth. Biol. 1, 130-138 (2012).
- S. C. Patel, M. H. Hecht, Directed evolution of the peroxidase activity of a *de novo*-designed protein. *Protein Eng. Des. Sel.* **25**, 445–452 (2012).
- K. M. Digianantonio, M. H. Hecht, A protein constructed de novo enables cell growth by altering gene regulation. Proc. Natl. Acad. Sci. U.S.A. 113, 2400-2405 (2016).
- K. M. Digianantonio, M. Korolev, M. H. Hecht, A non-natural protein rescues cells deleted for a key enzyme in central metabolism. ACS Synth. Biol. 6, 694-700 (2017).
- A. E. Donnelly, G. S. Murphy, K. M. Digianantonio, M. H. Hecht, A de novo enzyme catalyzes a lifesustaining reaction in Escherichia coli. Nat. Chem. Biol. 14, 253-255 (2018).
- J. A. Mancini et al., Design of a Fe 4 S 4 cluster into the core of a de novo four-helix bundle. Biotechnol. Appl. Biochem. 67, 574-585 (2020).
- M. S. Wang, M. H. Hecht, A completely de novo ATPase from combinatorial protein design. J. Am. Chem. Soc. 142, 15230-15234 (2020).
- Z. Yang et al., Biomanufacturing of CdS quantum dots. Green Chem. 17, 3775–3782 (2015).
- S. Stürzenbaum et al., Biosynthesis of luminescent quantum dots in an earthworm. Nat. Nanotechnol. 8, 57-60 (2013).
- H.-J. Bai, Z.-M. Zhang, Microbial synthesis of semiconductor lead sulfide nanoparticles using immobilized Rhodobacter sphaeroides. Mater. Lett. 63, 764-766 (2009).
- D. P. Cunningham, L. L. Lundie Jr., Precipitation of cadmium by Clostridium thermoaceticum. Appl. Environ. Microbiol. 59, 7-14 (1993).
- C. L. Wang, A. M. Lum, S. C. Ozuna, D. S. Clark, J. D. Keasling, Aerobic sulfide production and cadmium precipitation by Escherichia coli expressing the Treponema denticola cysteine desulfhydrase gene. Appl. Microbiol. Biotechnol. 56, 425-430 (2001).
- R. Dunleavy, L. Lu, C. J. Kiely, S. McIntosh, B. W. Berger, Single-enzyme biomineralization of cadmium sulfide nanocrystals with controlled optical properties. Proc. Natl. Acad. Sci. U.S.A. 113,
- L. C. Spangler, L. Lu, C. J. Kiely, B. W. Berger, S. McIntosh, Biomineralization of PbS and PbS-CdS core-shell nanocrystals and their application in quantum dot sensitized solar cells. *J. Mater. Chem. A* 4.6107-6115 (2016).
- 30. L. C. Spangler *et al.*, Enzymatic biomineralization of biocompatible CulnS₂ (CulnZn)S₂ and CulnS₂/ZnS consists for bioimaging. *Nanoscale* **9**, 9340-9351 (2017).
- S. Singh, K. Bozhilov, A. Mulchandani, N. Myung, W. Chen, Biologically programmed synthesis of core-shell CdSe/ZnS nanocrystals. *Chem. Commun.* **46**, 1473–1475 (2010).
- C. E. Flynn et al., Synthesis and organization of nanoscale II-VI semiconductor materials using evolved peptide specificity and viral capsid assembly. J. Mater. Chem. 13, 2414-2421 (2003).
- D. L. Feldheim, B. E. Eaton, Selection of biomolecules capable of mediating the formation of nanocrystals. ACS Nano 1, 154-159 (2007).

- 34. F. Liu et al., Enzyme mediated synthesis of phytochelatin-capped CdS nanocrystals. Appl. Phys. Lett. 97, 123703 (2010).
- Q. Sun et al., Structural basis for the inhibition mechanism of human cystathionine gamma-lyase, an enzyme responsible for the production of H₂S. J. Biol. Chem. 284, 3076-3085 (2009).
- T. Chiku et al., H₂S biogenesis by human cystathionine gamma-lyase leads to the novel sulfur metabolites lanthionine and homolanthionine and is responsive to the grade of
- hyperhomocysteinemia. *J. Biol. Chem.* **284**, 11601–11612 (2009).

 L. C. Spangler, J. P. Cline, C. J. Kiely, S. McIntosh, Low temperature aqueous synthesis of size-controlled nanocrystals through size focusing: A quantum dot biomineralization case study. Nanoscale 10, 20785-20795 (2018).
- R. Arai et al., Domain-swapped dimeric structure of a stable and functional de novo four-helix bundle protein, WA20. *J. Phys. Chem. B* **116**, 6789-6797 (2012).
- M. H. Stipanuk, I. Ueki, Dealing with methionine/homocysteine sulfur: Cysteine metabolism to taurine and inorganic sulfur. *J Inherit Metab Dis* **34**, 17–32 (2011).
- A. Sadeghnejad, L. Lu, C. J. Kiely, B. W. Berger, S. McIntosh, Single enzyme direct biomineralization of ZnS, Zn_xCd_{1-x}S and Zn_xCd_{1-x}S-ZnS quantum confined nanocrystals. RSCAdv. 7, 38490–38497
- A. Hoegl et al., Mining the cellular inventory of pyridoxal phosphate-dependent enzymes with functionalized cofactor mimics. Nat. Chem. 10, 1234-1245 (2018).
- J. Yang et al., Non-enzymatic hydrogen sulfide production from cysteine in blood is catalyzed by iron and vitamin B6. Commun. Biol. 2, 194 (2019).
- W. W. Yu, L. Qu, W. Guo, X. Peng, Experimental determination of the extinction coefficient of CdTe, CdSe, and CdS nanocrystals. *Chem. Mater.* **15**, 2854–2860 (2003).
- Z. Yang, L. Lu, C. J. Kiely, B. W. Berger, S. McIntosh, Biomineralized CdS quantum dot nanocrystals: optimizing synthesis conditions and improving functional properties by surface modification. Ind. Eng. Chem. Res. **55**, 11235–11244 (2016).
- M. K. Thorson, T. Majtan, J. P. Kraus, A. M. Barrios, Identification of cystathionine β-synthase inhibitors using a hydrogen sulfide selective probe. Angew. Chem. Int. Ed. 52, 4641-4644
- J. Jumper et al., Highly accurate protein structure prediction with AlphaFold. Nature 596, 583-589 (2021).
- D. L. Graham, M. L. Beio, D. L. Nelson, D. B. Berkowitz, Human serine racemase: Key residues/active site motifs and their relation to enzyme function. Front. Mol. Biosci. 6, 8 (2019).
- J. K. Choi et al., Chirality inversion of CdSe and CdS quantum dots without changing the stereochemistry of the capping ligand. ACS Nano 10, 3809-3815 (2016).
- M. P. Moloney, Y. K. Gun'ko, J. M. Kelly, Chiral highly luminescent CdS quantum dots. Chem. Commun. 3900-3902, (2007).
- R. Zhou, K.-Y. Wei, J.-S. Zhao, Y.-B. Jiang, Alternative chiral thiols for preparation of chiral CdS
- quantum dots covered immediately by achiral thiols. *Chem. Commun.* **47**, 6362 (2011). R. Xie, Z. Li, X. Peng, Nucleation kinetics vs chemical kinetics in the initial formation of semiconductor nanocrystals. J. Am. Chem. Soc. 131, 15457–15466 (2009).
- V. K. LaMer, R. H. Dinegar, Theory, production and mechanism of formation of monodispersed hydrosols. *J. Am. Chem. Soc.* **72**, 4847–4854 (1950).
- $Z.\,Yang,\,L.\,Lu,\,C.\,J.\,Kiely,\,B.\,W.\,Berger,\,S.\,McIntosh,\,Biomineralized\,\,CdS\,\,quantum\,\,dot\,\,nanocrystals:$ Optimizing synthesis conditions and improving functional properties by surface modification. Ind. Eng. Chem. Res. 55, 11235-11244 (2016).
- A. Priyam, A. Chatterjee, S. K. Das, A. Saha, Synthesis and spectral studies of cysteine- capped CdS nanoparticles. Res. Chem. Intermed. 31, 691-702 (2005).